Eddy-Driven Jet Sensitivity to Diabatic Heating in an Idealized GCM

HUGH S. BAKER, TIM WOOLLINGS, AND CHEIKH MBENGUE

Atmospheric, Oceanic and Planetary Physics, University of Oxford, Oxford, United Kingdom

(Manuscript received 2 December 2016, in final form 11 May 2017)

ABSTRACT

The eddy-driven jet is studied using a dry idealized model to determine its sensitivity to thermal forcings. The jet latitude, speed, and variability are investigated under a series of Gaussian patch thermal forcing simulations applied systematically on a latitude–sigma grid in the troposphere. This work builds on previous studies by isolating the responses of the jet speed and latitude as opposed to combining them into a single annular mode index. It also explores the sensitivity of the jet to much smaller spatial heatings rather than applying forcing patterns to simulate anthropogenic climate change, as the size and magnitude of the forcings due to anthropogenic climate change are uncertain. The jet speed and latitude are found to have different sensitivity distributions from each other, which also vary between summer and winter. A simple mechanistic understanding of these sensitivities is presented by considering how the individual thermal forcings modify mean isentropic surfaces. In the cases analyzed, the jet response to forcing scales approximately linearly with the strength of the forcing and when forcings are applied in combination. The findings show a rich latitude–pressure distribution of jet sensitivities to thermal forcings, which will aid interpretation of jet responses in a changing climate. Furthermore, they highlight the areas where uncertainty needs to be reduced in the size and position of expected anthropogenic forcings, in order that the uncertainty in changes of the eddy-driven jet can be reduced.

1. Introduction

The eddy-driven jet and associated storm track contribute to much of the weather and climate in the midlatitudes. Changes in the midlatitude eddy-driven jet stream latitude are one of the most robust circulation signs of climate change. Studies using the CMIP models find shifts, changes in amplitude, and changes in variability of the jets (Woollings et al. 2012; Barnes and Polvani 2013; Simpson et al. 2014; IPCC 2013). However, the magnitudes of these changes are uncertain (Grise and Polvani 2016) and the mechanisms unclear. Jet changes (both forced and due to internal variability) are a significant source of uncertainty in predictions of future regional climate (Karpechko 2010; Deser et al. 2012). Our inability to project the change in the jets thus limits our ability to quantify the effect of anthropogenic and natural forcings on the jets. Therefore, the degree to which weather and climate will be affected over regions such as northwestern Europe, and the real societal impact on those living in the midlatitudes, cannot yet be quantified. This makes it imperative to understand the response of the jets to forcing.

The response to anthropogenic climate change is multifaceted, involving complex interactions between many different systems. Moist processes should be considered when studying the eddy-driven jet (Shaw and Voigt 2015) and associated storm track (Shaw et al. 2016). However, since Mbengue and Schneider (2013) show that 80% of the storm track shift seen in CMIP5 simulations can be reproduced using a model with only dry dynamics, much can be learned about the response of the eddy-driven jets using a dry idealized model. Dry dynamical models are useful tools for understanding the response of the jets to heating, which in more complex systems may arise due to moist processes. Previous work has shown that idealized dry dynamical models (e.g., Lorenz and DeWeaver 2007; Butler et al. 2010; Mbengue and Schneider 2013; McGraw and Barnes 2016) do respond similarly to fully complex climate

Denotes content that is immediately available upon publication as open access.

Corresponding author: Hugh S. Baker, hugh.baker@physics.ox.ac.uk

DOI: 10.1175/JCLI-D-16-0864.1

models (e.g., Barnes and Polvani 2013; Simpson et al. 2014; Harvey et al. 2015). This suggests that an idealized model could be used to further investigate the sensitivity of the jets to forcing in different regions.

Many previous studies focus on the northern annular mode response to forcing (e.g., Lorenz and DeWeaver 2007; Ring and Plumb 2008). This fails to isolate the latitude shift from the changes in jet speed (Monahan and Fyfe 2006; Woollings et al. 2010). In this study, we use two distinct indices, one for jet speed and one for jet latitude. An alternative approach would be to use two or more EOFs (Vallis et al. 2004; Sheshadri and Plumb 2017). Studies that do separate the speed and latitude of the jet do so by applying forcings that are meant to mimic the expected forcings from anthropogenic climate change (e.g., Son and Lee 2005; Butler et al. 2010; Allen et al. 2012; Wang et al. 2012; Sun et al. 2013; Tandon et al. 2013; McGraw and Barnes 2016; Burrows et al. 2017). The shortfall here is that the exact anthropogenic forcing in the atmosphere is not known. This makes the results found in these studies highly dependent on the exact location and magnitude of the forcing applied. Sensitivity studies are important in this regard because, with a broader range of forcings, greater understanding of the possible response can be determined. In addition to climate change–like forcings, quantifying and characterizing jet sensitivities is also useful in understanding the response of the jets to natural variability such as the Atlantic multidecadal oscillation (Sutton and Dong 2012) and ENSO (Lu et al. 2008) and in assessing the sensitivity to model biases in the position of diabatic heating (Hawcroft et al. 2017). More generally, heating experiments such as this study can also be used in understanding the role of diabatic heating in modifying the atmospheric mean state (Hoskins and Valdes 1990) and its variability (e.g., Woollings et al. 2016).

There are a variety of mechanisms proposed to explain shifts in jet latitude. One theory is that changes in low-level baroclinicity can drive shifts in the storm track (Yin 2005; Brayshaw et al. 2008; Frierson 2008; Lu et al. 2010; Butler et al. 2011). Another theory states that changes in the upper troposphere and lower stratosphere modify wave propagation characteristics, leading to storm track shifts (e.g., Kushner and Polvani 2004; Chen and Held 2007; Butler et al. 2010). Chen et al. (2008) suggest that in the upper troposphere, an increase in meridional temperature gradient plays a key role in shifting the jet poleward. Lorenz and DeWeaver (2007) suggest that raising the tropopause height is responsible for a shift in the midlatitude jet, but the exact dynamical reason for this is as yet undetermined, suggesting also that near-surface changes in the meridional temperature gradient play a secondary role in the jet shift. However, Mbengue and Schneider (2017) show a near collocation between the maxima of near-surface eddy kinetic energy and near-surface extratropical temperature gradients in their climate change simulations, suggesting that near-surface meridional temperature gradients may play more than a secondary role. Other theories suggest that an increase in eddy length scales under global warming may contribute to storm track shifts (Kidston et al. 2010; Rivière 2011), that increased Rossby wave reflection of low phase speed waves across the jets act to cause the shift (Lorenz 2014), or that the effective diffusivity, as diagnosed using finite-amplitude wave theory, increases and advances upward and poleward, leading to a poleward displaced potential vorticity gradient peak in the upper troposphere (Lu et al. 2014).

This study investigates the sensitivity of the eddy-driven jet by applying a series of idealized thermal forcings to a simple GCM. We follow Lorenz and DeWeaver (2007) and Hassanzadeh and Kuang (2016) in applying localized perturbations systematically throughout the troposphere. We differ from their studies by evaluating the sensitivity of the different jet characteristics separately, and by applying finite-amplitude forcings (on the order of the magnitude of latent heating occurring in the atmosphere). This ensures a high signal-to-noise ratio but does not guarantee the linearity of the responses (see section 3c for linearity tests). In particular, the sensitivity to jet strength, position, and variability are determined. A large source of uncertainty in the response of the jet to climate change arises from the competing effects of tropical upper tropospheric heating and Arctic amplification. Developing an understanding of the sensitivity of the jet to these competing influences allows the response of the jet to be quantified more accurately.

Idealized modeling studies find that the response of the jet is not uniform across all seasons (e.g., Butler et al. 2010; McGraw and Barnes 2016). Seasonal variations in jet responses are also found in CMIP5 (Simpson et al. 2014). These changes in the jet appear to have an important contribution from changes in low-frequency/stationary waves but the mechanisms are not yet well understood. In our idealized simulations, the meridional near-surface radiative-equilibrium temperature profile is set so that the resulting temperatures mimic a North Atlantic wintertime and summertime temperature profile in the Southern and Northern Hemisphere, respectively.

The focus of this work is on the jet sensitivity to tropospheric forcings. There is evidence that stratospheric dynamics and coupling to the troposphere can influence the eddy-driven jet (e.g., Polvani and Kushner 2002; Gerber and Polvani 2009; Son et al. 2009; Manzini et al. 2014). Given the potential complexity of stratosphere–troposphere interactions (Mitchell et al. 2013), a much

more realistic model might be needed to assess the stratospheric sensitivities. Here the model does not attempt to reproduce the dynamics seen in the stratosphere, allowing the sole focus to be on the tropospheric dynamics.

The storm tracks are intimately connected via eddy fluxes to the jet. Using eddy flux quantities to quantify the sensitivity of the storm track, greater understanding of how the jet shifts occur is developed. Section 2 outlines the methods used to investigate the jet and storm track sensitivities including the model setup and experimental design. Sensitivity results are presented in section 3, along with an in-depth look at four case study simulations to further understand the dynamics behind the sensitivities. A series of diagnostics are used to understand the sensitivities that these simulations produce. This section also explores the linearity of the responses to the amplitude of the forcing, and to combinations of forcings. Some existing theories are tested in section 4 to determine whether the sensitivities determined by this study corroborate those theories from previous studies. Finally, the conclusions are presented in section 5.

2. Methods

a. Model

Simulations are conducted using the Geophysical Fluid Dynamics Laboratory's Flexible Modeling System dry dynamical core. The model solves the equations of motion using a spectral transform method at T42 resolution with 37 unevenly spaced sigma levels. Temperatures are relaxed to a zonally symmetric radiative-equilibrium thermal profile. A quasi-equilibrium convection scheme relaxes temperatures to a prescribed lapse rate $\gamma\Gamma_d$, where Γ_d is the dry adiabatic lapse rate (g/c_p) and γ is a number between 0 and 1. Here, $\gamma = 0.7$ is used. Vertical diffusion of momentum and dry static energy acts within the boundary layer up to 2.5 km. A full description of the model used can be found in Schneider and Walker (2006). The simplistic setup makes it possible to perform long ensemble simulations without being computationally intensive.

Temperatures are relaxed toward radiative equilibrium on a time scale of 7 days near the surface at low latitudes and 50 days in the rest of the atmosphere. The surface temperature in radiative equilibrium varies with latitude ϕ as

$$T_s^e(\phi) = \tilde{T}_s^s + \Delta_h[\cos^2\phi + 2\sin\phi_0(1+\sin\phi)], \quad (1)$$

where $\tilde{T}_s^e = 230$ K is the surface temperature at the south pole, $\Delta_h = 95$ K is the pole–equator thermal contrast, and $\phi_0 = 10°$ is the latitude of maximum solar irradiance. Aside from this altered surface temperature profile, the model setup is that of Schneider and Walker (2006). The radiative-equilibrium profile is detailed below for completeness. The radiative equilibrium temperature away from the surface is given by

$$T^e(\phi, p) = T_t^e\left[1 + d_0(\phi)\left(\frac{p}{p_0}\right)^{\alpha}\right]^{1/4}, \quad (2)$$

where

$$d_0(\phi) = \left[\frac{T_s^e(\phi)}{T_t^e}\right]^4 - 1, \quad (3)$$

and

$$d = d_0(\phi)\left(\frac{p}{p_0}\right)^{\alpha} \quad (4)$$

is a latitude-dependent optical thickness that depends on the near-surface radiative equilibrium temperature $T_s^e(\phi)$ (Schneider 2004). The constant $p_0 = 1000$ hPa is a reference surface pressure, and the exponent $\alpha = 3.5$, the ratio of the pressure scale height to the partial pressure scale height of the dominant infrared absorber (e.g., water vapor on Earth), controls the lapse rate of the radiative equilibrium state. The optical thickness is chosen so that the radiative equilibrium temperature T_t^e at the top of the atmosphere is constant. In this study, $T_t^e = 200$ K, assuming that a fixed longwave emission temperature for a gray atmosphere is proportional to the temperature at the top of the atmosphere (Schneider 2007).

All simulations use the values for the parameters in (1), which have been explicitly chosen to create a state that mimics the North Atlantic. This creates a background state with a winter hemisphere and summer hemisphere with conditions generally resembling those from reanalysis data. Figure 1 compares the temperature at the lowest model level in a statistically steady state to surface temperature data taken from the NCEP–DOE Reanalysis (NCEP Reanalysis 2 data provided by the NOAA/OAR/ESRL PSD, Boulder, Colorado, from their website at http://www.esrl.noaa.gov/psd/), time averaged from 1979–2015 and averaged over the North Atlantic region 0°–60°W, showing they are in good agreement with each other. The North Atlantic state is chosen, rather than a zonal mean state, in order to represent an ocean storm track system. Therefore, while the background state resembles the North Atlantic, the results in this study apply more generally to ocean storm tracks.

The model is run in perpetual winter (SH) and summer (NH) conditions with no diurnal or seasonal cycle. Horizontal hyperdiffusion, ∇^8, damps the smallest resolved

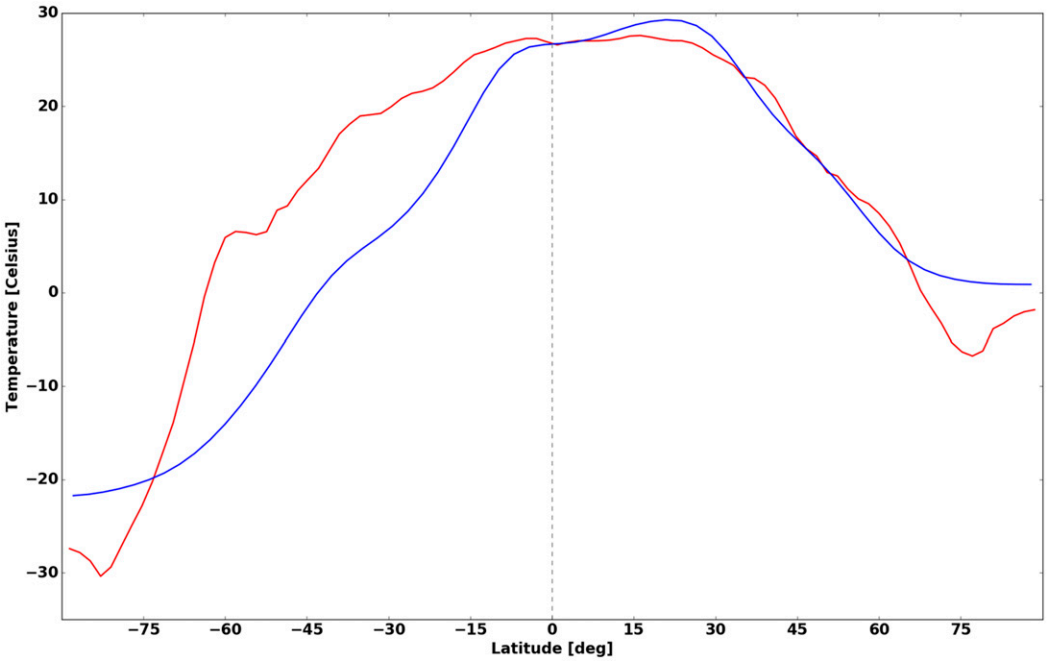

FIG. 1. Comparison of reanalysis (red) and model (blue) surface temperature. The dashed gray line shows where the winter and summer reanalysis data over the North Atlantic have been stitched together, such that the left half of the figure shows winter data and the right half shows summer data. Model output is the temperature of the lowest model level taken from a 6-yr control simulation. The reanalysis surface temperature data are taken from the NCEP–DOE reanalysis time averaged from 1979 to 2015 and averaged over the North Atlantic region 0°–60°W.

scales. In addition, there are no continents or ocean, and no zonal asymmetries to excite stationary waves. Idealized modeling studies with no topography and/or low resolution often produce jets with too persistent annular modes (e.g., Gerber and Vallis 2007; Gerber et al. 2008; Gerber and Polvani 2009; Chan and Plumb 2009). In our setup, the decorrelation time scale [calculated using the *e*-folding time, as in Baldwin et al. (2003)] of the jet indices in the control simulation are 7.4 and 9.6 days for the winter and summer jet latitudes, respectively. These time scales are on the same order of magnitude as those found in Keeley et al. (2009) for the NAO (their Fig. 1) of 10 and 5 days for winter and summer respectively.

b. *Control simulation*

A spinup is run for 10 years to allow the model to reach a statistically steady state, and then a 6-yr control simulation is performed. A comparison of the zonal mean zonal wind, $\overline{u}$, with the reanalysis data, time averaged from 1979–2015 and averaged over the North Atlantic region 0°–60°W, is displayed in Fig. 2. The model qualitatively reproduces the zonal wind field seen in the reanalysis, with the jets at a similar latitude to the reanalysis; both model jets are stronger than the reanalysis jets, but with similar broad structure. This discrepancy in strength could arise for several reasons. With no ocean transport in the model, the eddies must be stronger than in the reanalysis in order to transport the same amount of heat poleward to reproduce the temperature profile seen in the reanalysis. The winter jet in the model is stronger than observed because the maximum near-surface temperature gradient in the baroclinic zone of the model is larger. There are also no stationary eddies and no moisture in the model. Moisture allows more poleward energy transport through latent transport for the same divergent circulation strength. The lack of topography could also cause this discrepancy in strength (compare the stronger austral jets to the weaker boreal jets). The subtropical jets are visible on the equatorward flank of the eddy-driven jets. Note that the summer jet displays a slight poleward bias in its position, similar to most GCMs including the CMIP suite, which often display poleward biases of up to 5° in the summer jet latitude (Hannachi et al. 2013).

Jet indices are defined for the strength and position of the jet using the maximum of the zonally averaged zonal wind at $\sigma = 0.85$. The height is chosen to be just above the model boundary layer but low enough to separate the eddy-driven jet from the subtropical jet (which has its maximum around $\sigma = 0.2$). The maximum is found by fitting a second-order polynomial around the maximum of zonal wind at $\sigma = 0.85$ in each hemisphere, and taking

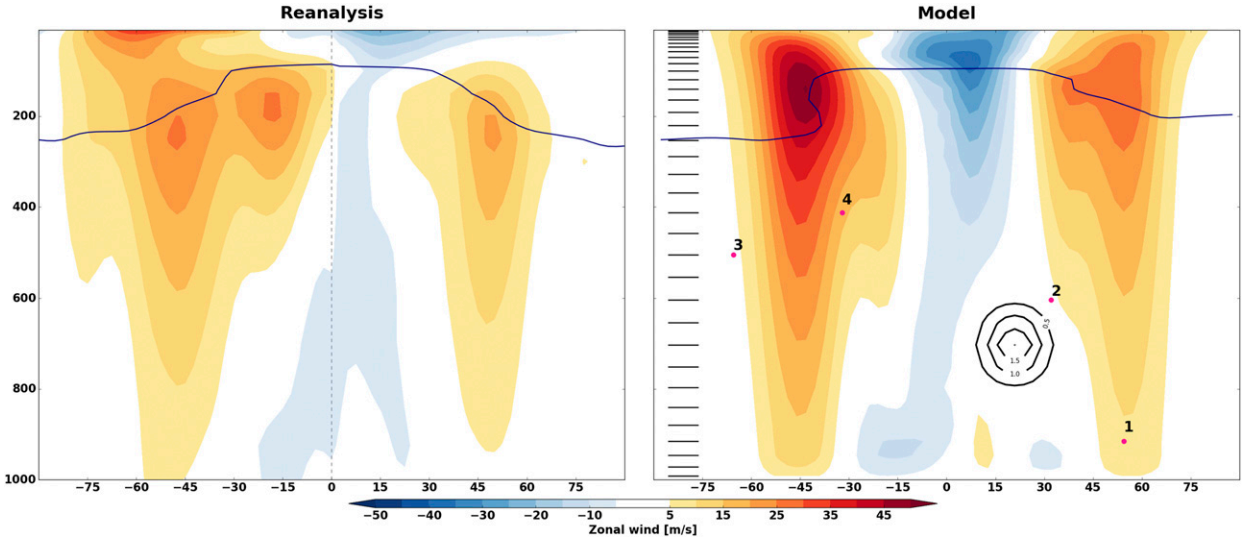

FIG. 2. Comparison of $\overline{u}$. The blue line indicates the tropopause, computed as the sigma level at which the lapse rate $\Gamma = 2\,\mathrm{K\,km^{-1}}$, the WMO criterion. The dashed gray line shows where the winter and summer reanalysis data over the North Atlantic have been stitched together, such that the left half of the figure shows winter data and the right half shows summer data. Model output is taken from a 6-yr control simulation. The reanalysis data are taken from the NCEP–DOE reanalysis time averaged over 1979–2015 and averaged over the North Atlantic region 0°–60°W. Also shown in black are the model levels. A sample heating is plotted in the black contours to show the spatial extent of the forcings applied. Pink dots indicate the locations of the case studies.

the maximum of the polynomial fit as the jet strength and its latitude as the jet position. Throughout the study we refer to changes in the eddy-driven jet as the changes in the maximum of the zonal mean zonal wind at $\sigma = 0.85$; subtropical jet changes have not been investigated. Storm track indices are also defined using two different measures: $\overline{v'T'}$ taken at $\sigma = 0.85$ and $\nabla \cdot \overline{u'v'}$ at $\sigma = 0.25$ (primed quantities represent deviations from the time mean, and the overbar indicates a zonal and temporal average).

c. *Heating experiments*

Tropospheric thermal forcings are applied in a series of 306 heating experiments. The forcings are zonally uniform and are applied in the latitude–sigma plane, across 34 different latitudes and at 9 sigma levels, and are held constant over the length of the simulation. The forcings are applied as a diabatic source term via a Gaussian patch with heating following Hassanzadeh and Kuang (2016), given by

$$\mathscr{H}(\phi,\sigma) = q_0 \exp\left\{-\left[\frac{(\phi-\phi_0)^2}{2\chi_\phi^2} + \frac{(\sigma-\sigma_0)^2}{2\chi_\sigma^2}\right]\right\}. \quad (5)$$

Here, ϕ and σ represent the latitude (in radians) and the sigma level respectively. For each simulation the heating is applied at coordinates (ϕ_0, σ_0). In all simulations, the magnitude of the heating is given by $q_0 = 2\,\mathrm{K\,day^{-1}}$, and the spatial size of the heating is determined by $\chi_\phi = 0.12341$ rad, $\chi_\sigma = 0.053$ (an example of the heating is shown in Fig. 2). The spatial size of the patches used is taken from Hassanzadeh and Kuang (2016), where a series of simulations across the latitude–sigma plane in the linear regime are conducted, in order to build a linear response function. The magnitude of the forcing that Hassanzadeh and Kuang (2016) use varies with position to ensure all simulations are within the linear regime. In this study, the magnitude of the forcing is kept constant at $2\,\mathrm{K\,day^{-1}}$, a similar order of magnitude to Hassanzadeh and Kuang (2016) (who use forcings varying from 0.1 to $3.5\,\mathrm{K\,day^{-1}}$), to ensure the sensitivities that are found are all to an equal magnitude of forcing. A similar set of simulations run with $q_0 = 0.5\,\mathrm{K\,day^{-1}}$ (not shown) produced very similar patterns of sensitivity (see section 3a) as with $q_0 = 2\,\mathrm{K\,day^{-1}}$. The value $q_0 = 2\,\mathrm{K\,day^{-1}}$ is used to give a larger response signal; as shown for specific case studies in section 3c, the response of the jet to varying magnitude of thermal forcing is approximately linear, and so there are no linearity issues with using the larger forcing. While the amplitude of the forcing used here is greater than that used in Butler et al. (2010) ($q_0 = 0.5\,\mathrm{K\,day^{-1}}$), the spatial extent is substantially smaller, and so the forcings produce temperature changes of a similar maximum amplitude to those of Butler et al. (2010) (not shown).

All simulations are started from the end of the 10-yr spinup period. For each simulation, the patch is then

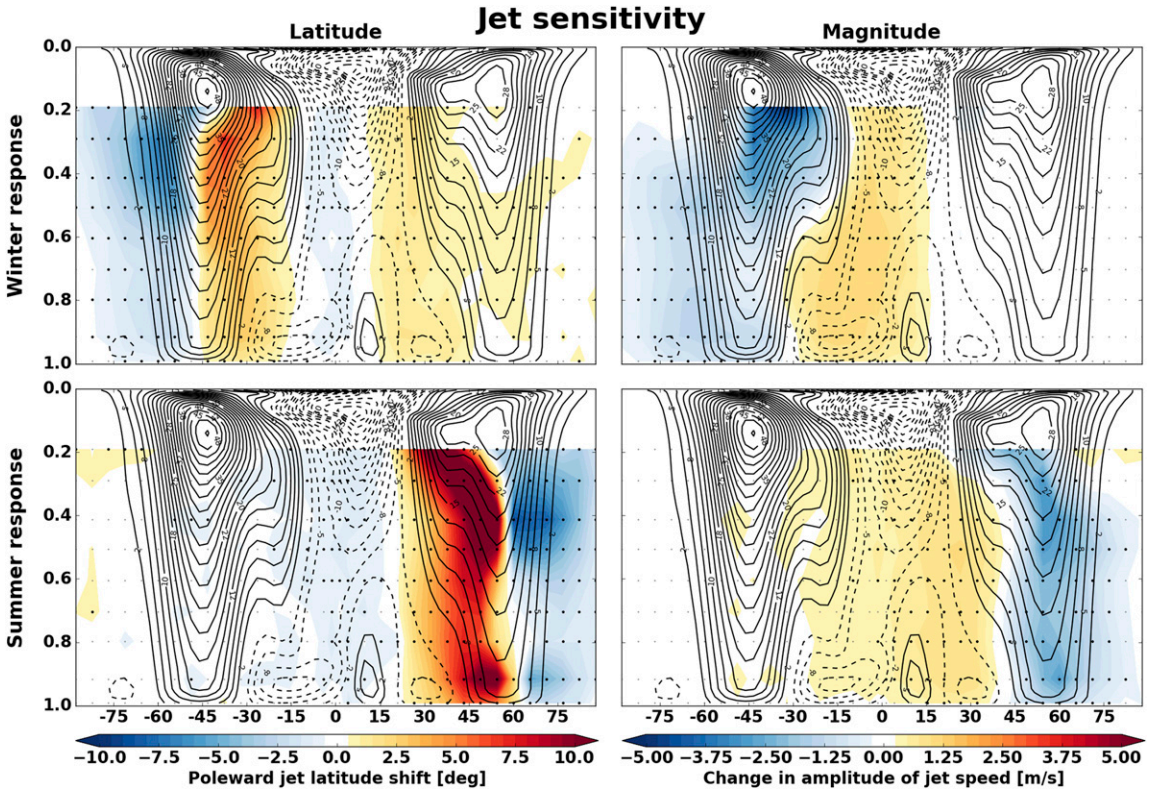

FIG. 3. Sensitivity of the jet indices to heating experiments (colors) in the latitude–sigma plane. Contours indicate the control $\overline{u}$. The black dots mark where the difference between the control and perturbed simulations is statistically significantly different from the control, while the gray dots show where the difference is not statistically significant. Positive values correspond to poleward shift or strengthening of the jet in the target hemisphere (top: winter; bottom: summer).

applied, and a further year is run before collecting 6 years of model output. From each simulation, $\overline{u}$ is used to calculate the jet indices, and the sensitivity is determined from the difference in the jet indices from the control simulation. Following Woollings et al. (2008), statistical significance in the sensitivity is estimated using the daily jet indices by applying a two-tailed t test at the 99% confidence level. Each time series has an effective sample size:

$$N_i^{\text{eff}} = N\left(\frac{1-\rho_i}{1+\rho_i}\right), \tag{6}$$

where N is the actual sample size and ρ_i is the lag-1 autocorrelation coefficient of the time series. The t statistic is calculated as

$$t = \frac{\mu_i - \mu_j}{\sqrt{\dfrac{\sigma_i^2}{N_i^{\text{eff}}} + \dfrac{\sigma_j^2}{N_j^{\text{eff}}}}}, \tag{7}$$

where μ_i is the mean of time series i and σ_i is the standard deviation.

3. Results

a. Sensitivities

Figure 3 summarizes all the simulations by showing sensitivities of the jet indices to heating in all regions. The shading at a given point quantifies the change in the jet when heating is applied at that location. The change in the winter jet is measured in the upper panels, and the change in the summer jet in the lower panels. In all figures, the left-hand hemisphere (negative latitudes) is the winter hemisphere and the right-hand hemisphere (positive latitudes) is the summer hemisphere. For example, when a thermal forcing is applied at $\sigma = 0.8$ and $\phi = 30°$ (a forcing in the summer hemisphere), Fig. 3 shows that both the winter jet (top panels) and summer jet (bottom panels) shift poleward, with a strengthening of the summer jet. The control zonal mean zonal wind is contoured for orientation. It is immediately apparent that the latitude and speed of the jet have different sensitivity distributions. This highlights the need to consider the two indices separately, unlike in the annular mode and NAO frameworks. For the idealized GCM, the annular mode change (not shown) is mostly reflective of the jet latitude shift.

The largest response in the latitude of the jet in both summer and winter comes from heating on the flanks of the jet core. About the jet core, the response is highly sensitive to the position of the heating; heating equatorward of the core shifts the jet poleward, and heating poleward of the core shifts the jet equatorward. The latitude sensitivity of the summer jet is confined to the region close to the jet, whereas the winter jet shifts poleward due to heating in the subtropics of either hemisphere. The climatological jet position has been shown to impact its response to external forcing (e.g., Garfinkel et al. 2013; McGraw and Barnes 2016). The climatological jet is farther poleward in summer due to the seasonal cycle, and so the response of the jet latitude is less sensitive to heating in the tropics, but more sensitive to heating at the pole. This is in agreement with the work of Petrie et al. (2015), where a response to sea ice loss in the Arctic is found to drive an equatorward shift in the summer jet, but with no significant change in winter. Changes in jet latitude in winter due to polar heating near the surface still elicit an equatorward jet shift, as found in Kim et al. (2014) and Sun et al. (2015), for example. It should be noted that, under anthropogenic climate change, the heating due to sea ice loss in the Arctic is expected to be larger in winter (Deser et al. 2010), and so whether a greater jet shift might be seen in summer or winter depends on the two factors: jet sensitivity and amplitude of forcing.

Heating over the pole weakens the jet, although the additional change in jet latitude shows that the response is more complicated than a simple weakening of the jet, as in Francis and Vavrus (2012), for example, who just consider a weakening of the jet with no change in jet latitude. In the deep tropics, heating affects the strength of the jet to a far greater degree than the latitude of the jet, with jet shifts less than 1° until the forcing is farther than 15° from the equator. In general, heating equatorward of the midlatitude westerlies and throughout the tropics produces a jet strengthening, and heating in the midlatitude westerlies and farther poleward produces a weakening. Note the offset between the change of sign of sensitivity of the latitude and magnitude of the jet; the latitude shift changes sign about the core of the jet, whereas the magnitude response changes sign on the equatorward flank of the westerlies. This suggests that for a range of forcing the jet shifts poleward and weakens.

Heating at different levels generally gives the same sign of response, and the sensitivity often increases with height up to around $\sigma = 0.4$ in the midlatitudes. This could be due to changes in static stability, as heating higher in the atmosphere will increase the stability in the storm track region below the heating. Another reason could be due to near-surface friction affecting eddy amplitudes and leading to differences between simulations with heating in the lower troposphere and the upper troposphere (Held 2007). However, neither of these two mechanisms is confirmed, especially as the sensitivity with height mainly affects the latitude shifts and not the changes in magnitudes. Above $\sigma = 0.4$, the heating has the potential to significantly alter the tropopause height, affecting the dynamics. There is also a peak in the amplitude of the response when the heating is applied at $\sigma = 0.9$ near to the jet core, especially prevalent in the summer hemisphere. These sensitivities are explored in the *case studies* subsection.

To allow comparison with the jet sensitivities, storm track sensitivity maps are plotted using the two measures defined, $\overline{v'T'}$ and $\nabla \cdot \overline{u'v'}$ (Figs. 4 and 5). There is a broad agreement between the sensitivity of the jet and storm track; for the magnitude of the forcing used in this study, local heating is needed to affect the storm track position, whereas the magnitude is sensitive to heating in the tropics as well. As with the jet sensitivities, the magnitude of the storm track is more sensitive in winter, and the latitude more sensitive in summer. These contrasts potentially arise from differences in the magnitude of the temperature gradients in the two hemispheres. The climatological maximum of $\overline{v'T'}$ is offset slightly equatorward of the climatological $\overline{u}$ maximum. The maximum magnitude of $\nabla \cdot \overline{u'v'}$ is offset slightly poleward of the $\overline{u}$ maximum. This may help to explain the difference in position of the latitude where the sensitivity of the magnitude and latitude shifts changes sign. Heating on the equatorward flank of the jet lies on the region of maximum $\overline{v'T'}$. Hence heating here acts to push the temperature gradient, and hence $\overline{v'T'}$ maximum, farther poleward. Heating either side of the $\overline{v'T'}$ maximum will give changes in the strength of the temperature gradient and hence changes in the magnitude of $\overline{v'T'}$. The strong jet weakening in response to upper-level heating on the equatorward jet flank is accompanied by a strong weakening of the storm track. This is likely due to the increased static stability below the heating, which in this case lies directly over the $\overline{v'T'}$ maximum.

The change in variability, or the spread of the distribution of the jet latitude and speed, is assessed by considering the change in standard deviation of the indices. For each simulation, the daily time series of jet indices are used to calculate the standard deviation of the jet speed and latitude. The change in spread is calculated by subtracting the control standard deviation from the forced simulation standard deviation. Figure 6 shows the sensitivities of the spread of the jet indices in response to the thermal forcings. To affect the jet spread by an appreciable amount, thermal forcing must be applied outside the tropics. The greatest increase in variability comes from heating inside the jet core and on the equatorward

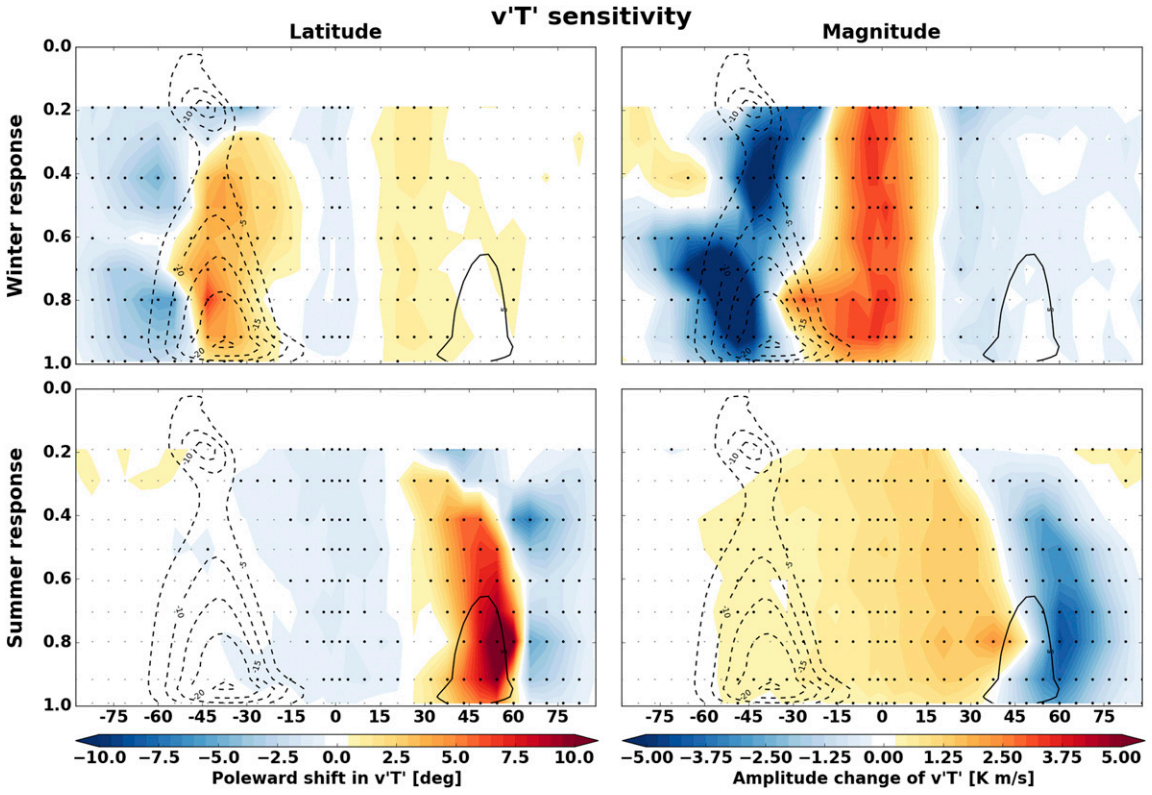

FIG. 4. As in Fig. 3, but for $\overline{v'T'}$. Positive values correspond to poleward shift or an increasing of the amplitude of $\overline{v'T'}$ in the target hemisphere.

flank of the jet, causing an increase in both jet speed and latitude spread. There are no locations where the thermal forcing causes a decrease in the winter jet latitude spread. However, for the jet speed in winter, and both latitude and speed in summer, heating on the poleward flank of the jet and over the poles causes a decrease in the spread of the jet latitude and speed.

Barnes and Hartmann (2011) use a barotropic model to show the leading mode of variability transitions from a shift to a pulse as the jet is shifted poleward, implying a decrease in jet latitude spread. This does not support our findings that the jet latitude spread increases as the jet is shifted poleward. However, Barnes and Hartmann (2011) also show that as the eddy-driven jet moves away from the subtropical jet, the leading mode of variability of the eddy-driven jet shifts from a pulsing mode to a meridional shifting mode. In our simulations, we may be seeing a combination of these two effects influencing the jet spread. McGraw and Barnes (2016) use a dry idealized model to show the spread of the jet strength increases as the jet is shifted poleward, in agreement with our findings. Our findings are also in agreement with, for example, Kidston and Gerber (2010) and Burrows et al. (2017), who note a decrease in persistence time for a poleward shifted jet.

The increase in spread on synoptic time scales may result from increases in the mean meridional temperature gradient or the width of the baroclinic zone. Consider the baroclinic zone width in a simplified case. Take the baroclinic zone as occurring in the region with a strong meridional temperature gradient, with the jet at the latitude of steepest temperature gradient. In general, a heating on the equatorward side of the jet acts to increase the mean temperature gradient and, due to an increase in available potential energy that increases the amount of eddy activity, an increase the baroclinic zone width. Both the increase in mean temperature gradient and the increase in baroclinic zone width may act to increase the spread of jet latitudes and magnitudes. In contrast, a heating poleward of the jet acts to reduce the extent in the baroclinic zone width and mean temperature gradient, thus reducing the spread of jet latitudes and magnitudes.

b. *Case studies*

To investigate the mechanisms behind the shifts and strengthening of the jet discussed above, it is instructive to consider a series of case studies displaying different behavior due to the location of the thermal forcing (case study forcing locations displayed in Fig. 2).

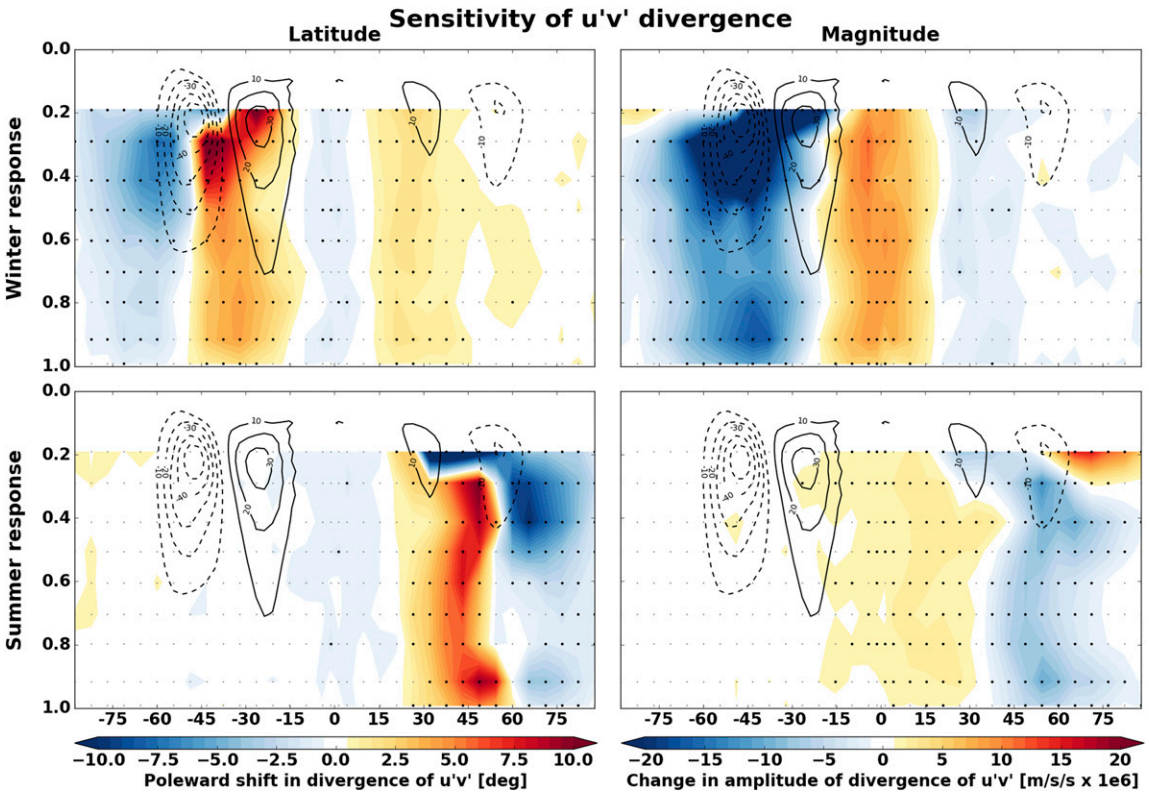

FIG. 5. As in Fig. 3, but for $\nabla \cdot \overline{u'v'}$. Positive values correspond to poleward shift or an increasing of the amplitude of $\nabla \cdot \overline{u'v'}$ in the target hemisphere.

The first of these, displayed in Fig. 7, examines the response to near-surface heating in the region of large summer jet latitude response (pink dot). Here, the forcing causes a poleward shift of the summer jet latitude, but a decrease in its speed. The thermal forcing weakens the low-level meridional temperature gradient in summer and shifts the location of the steepest isentropes poleward. This acts to weaken $\overline{v'T'}$ and to shift it poleward, causing the weakening and shift of the jet. Changes in jet speed may be mediated via the following mechanism: a decrease in $\overline{v'T'}$ causes a downward EP flux anomaly, which in turn weakens upper-level momentum fluxes. The weakened poleward heat transport also acts to set up an anomalous overturning circulation, with the lower branch moving equatorward. The Coriolis effect then turns this equatorward-moving air toward the west, thus weakening the lower-level westerly winds and hence the jet, as in Edmon et al. (1980). For an increase in jet speed, a strengthening in $\overline{v'T'}$ sets off the same cycle, but with opposite signs. This forcing is between the maxima of $\overline{v'T'}$ and $\overline{u}$, causing a weakening but poleward shift of the jet. More commonly, a poleward shift of the jet would be associated with the jet strengthening [due to eddy phase speed arguments such as in Chen and Held (2007)]. Heating above this level is above the maximum in $\overline{v'T'}$, and so the responses are weaker until they begin to strengthen again up toward $\sigma = 0.4$, as discussed in section 3a.

In the second example, displayed in Fig. 8, the summer jet responds to the midtropospheric subtropical forcing by strengthening and shifting poleward, and the winter jet shifts poleward (see Fig. 3). The heating is now equatorward of the maximum in meridional heat flux and thus $\overline{v'T'}$ strengthens, causing an acceleration of the jet as described above. The isentropes steepen poleward of the heating, causing the jet to shift poleward to the steeper region. The effect on the winter jet arises as the thermal forcing modifies global isentropes, conveying the shift in jet latitude through the overturning circulation. An increase in interhemispheric energy asymmetry leads to a stronger cross-equatorial flow, with the ascending branch of the Hadley cell displaced into the summer hemisphere. The Hadley cell, which relaxes temperature gradients in the deep tropics toward zero, communicates changes in the summer hemisphere to the winter hemisphere through a modification of the temperature gradients in the winter hemisphere. This effect occurs due to subtropical heating in summer hemisphere, where the Hadley cell acts to transport the

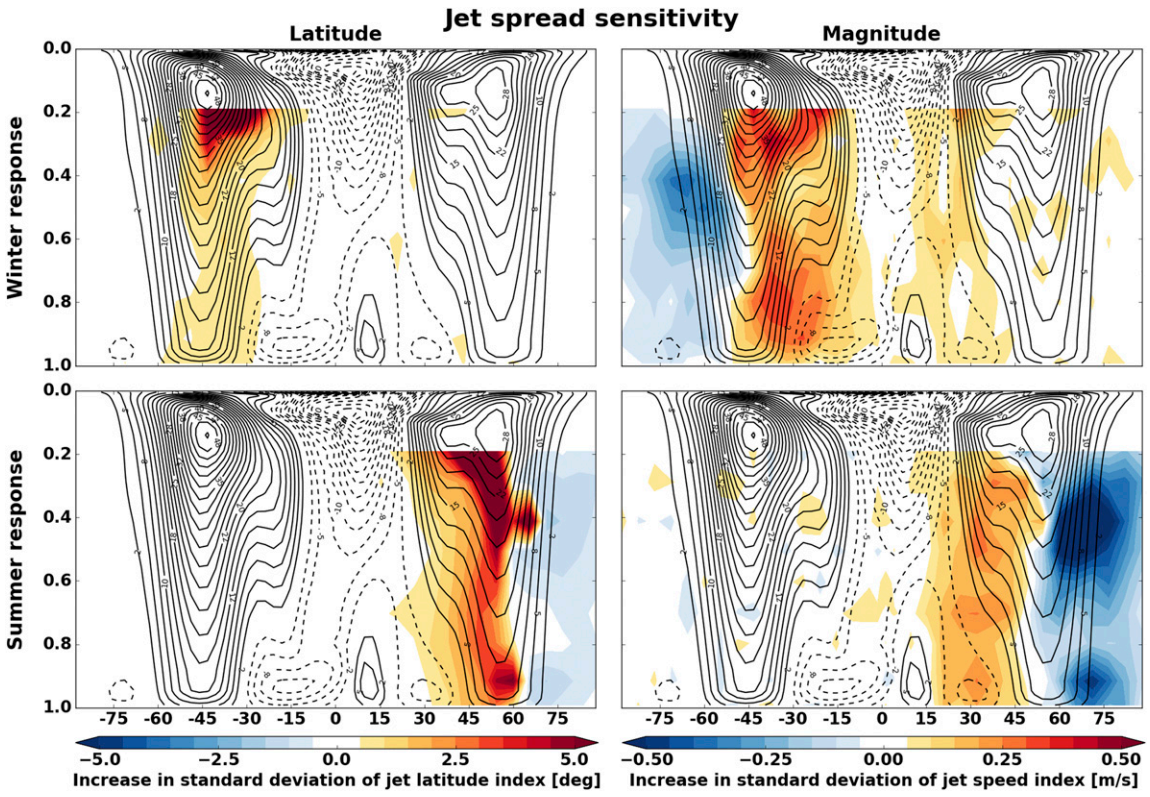

FIG. 6. As in Fig. 3, but for jet spread. Positive values correspond to an increase in spread of the jet position or strength in the target hemisphere.

energy into the winter hemisphere. Heating at the same latitude in the winter hemisphere, however, does not produce an effect on the summer jet as then the heating would reduce the Hadley circulation strength.

The third case study examines midtropospheric heating on the poleward flank of the winter jet (Fig. 9). This causes a flattening of the isentropes at the latitude where the heating is applied, shifting the maximum of the baroclinic zone equatorward and contracting the baroclinic zone, thus shifting the jet equatorward. The low-level temperature gradient across the jet weakens, weakening the eddy transports and thus weakening the jet via thermal wind balance. Heating at the same latitude but higher in the atmosphere (not shown) creates a region of high static stability below the heating, thus compressing the local isentropes, which acts to flatten the near-surface isentropes causing an equatorward shift of the mean temperature gradient, shifting the jet farther equatorward. Heating at the same level, but farther equatorward, acts to greatly weaken the low-level meridional temperature gradient and the momentum fluxes on the equatorward flank of the jet (not shown), causing a greater weakening of the jet.

The final case study looks at the response to a midtropospheric midlatitude forcing on the equatorward flank of the winter jet (Fig. 10). A poleward shift in the jet arises due to the latitude of steepest isentropes shifting poleward, which acts to shift $\overline{v'T'}$ poleward. However, the low-level meridional temperature gradient weakens, causing $\overline{v'T'}$ to weaken, giving a weakening of the jet via the same mechanism as in the first case study. Thermal forcings at the same level, but moving closer to the equator progressively, act less to weaken the low-level meridional temperature gradients. Once past a critical latitude, the thermal forcing begins to act to increase the low-level meridional temperature gradients, thus causing the strengthening of the jets seen for forcings in the tropics.

By considering the four case studies, it is apparent that many of the jet shifts seem to be associated with meridional shifts in the maximum low-level meridional temperature gradients, shifting the position in maximum meridional heat flux. Jet speed changes seem to be associated with changes in the magnitude of the low-level meridional temperature gradients, which lead to changes in $\overline{v'T'}$ relative to the climatological maximum.

Because of the number of simulations, it is unfeasible in this study to examine the mechanisms by which the jet responds in all simulations, and it is possible that other mechanisms are at play in the other heating simulations.

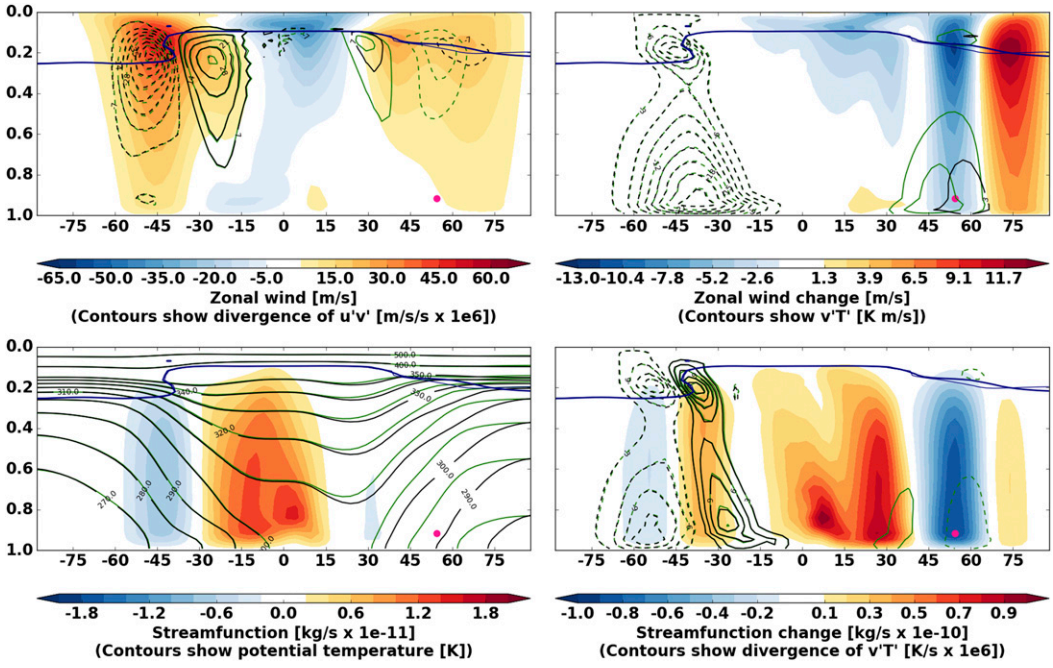

FIG. 7. Case 1: Summary plot for heating applied at $\sigma = 0.9$ and $\phi = 54°$ (pink dot). (top left) Simulation $\overline{u}$ (colors), $\nabla \cdot \overline{u'v'}$ (black contours for simulation, green for control). (top right) Change in $\overline{u}$ (colors), $\overline{v'T'}$ (black contours for simulation, green for control). (bottom left) Simulation streamfunction (colors), potential temperature (black contours for simulation, green for control). (bottom right) Change in streamfunction (colors), $\nabla \cdot \overline{u'v'}$ (black contours for simulation, green for control). The thick blue line is the tropopause in the simulation and the thin blue line is the control tropopause.

All results considered in this study concern the fully equilibrated response. Some spinup ensemble simulations, similar to those of Sun et al. (2013), have been performed for the four case studies using a 200-member initial condition perturbation ensemble (not shown). Heating is applied at day zero and the ensemble mean response at each day is used to investigate the mechanisms of how the jet responds to the heating. Changes in $u'v'$ associated with upper-level wind changes are observed. However, the response is apparent earliest in $\overline{v'T'}$, suggesting that in the ensemble, changes in baroclinic growth are instrumental in initiating the jet response. We leave it to a future study to investigate exactly how these responses are set up.

c. *Linearity of simulations*

To determine whether the response of the jet to the forcings behaves linearly, two further sets of simulations are run. The first of these varies the strength of the thermal forcing at each of the four heating locations used in the case studies. The term q_0 is set to 0.1, 0.5, 1.0, 1.5, 2.0, and 2.5 K day^{-1}, and the resultant changes in jet indices are plotted in Fig. 11. In the regime of heating between 0 and 2.5 K day^{-1}, the response to forcing in both the jet speed and position, summer and winter, is approximately linear. It should be noted that for the stronger heatings there are some instances where the response of the summer jet latitude does deviate from linearity.

In the second test of linearity, the forcings applied in each of the individual case studies are applied in all possible combinations and simulated as in the original sensitivity simulations. Figure 12 displays the change in jet index in each combined simulation against the sum of the changes in jet indices from the respective individually forced simulations. Aside from the summer responses in simulations that include the forcings in the first two case studies, the results are also approximately linear. The responses to simulations that do contain the forcings from the first two case studies display smaller-amplitude responses than in their respective linear combinations, which is possibly due to the proximity of the two forcings and the similar mechanism by which they affect the summer jet, or possibly to the fact that the limit of linearity has been reached. Note, of course, that only a few test cases have been combined in this study, and in some scenarios we are combining forcings from opposite hemispheres.

These linearity tests demonstrate that, for the case studies tested, the jet response to forcing scales

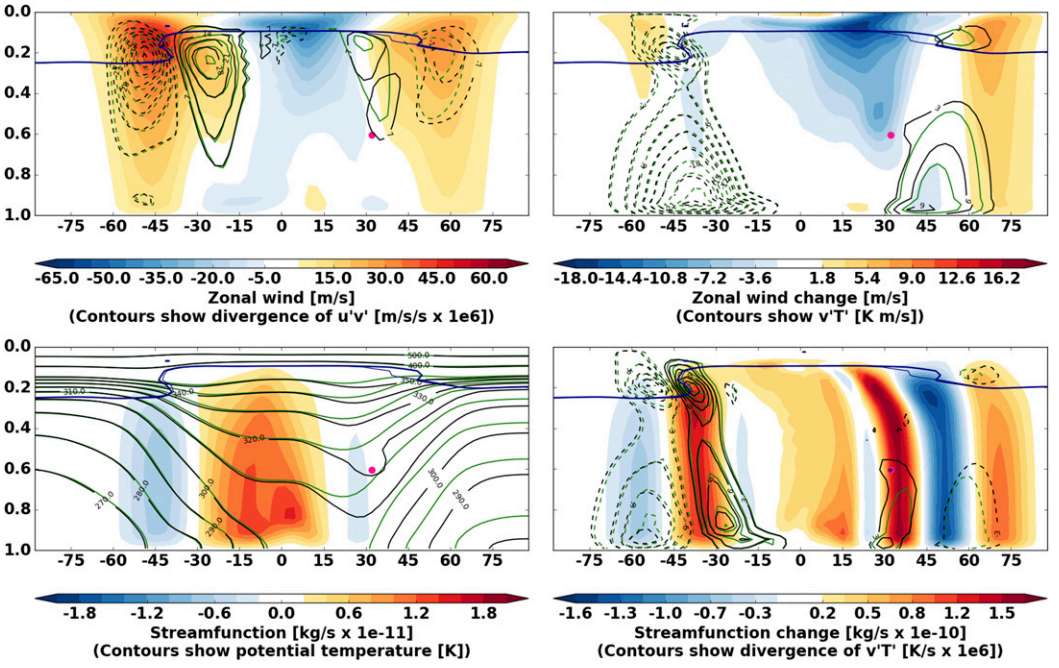

FIG. 8. Case 2: As in Fig. 7, but for heating applied at $\sigma = 0.6$ and $\phi = 32°$ (pink dot).

approximately linearly with the strength of the forcing, and when forcings are applied in combination. As noted in Tandon et al. (2013), who applied a similar amplitude (but larger spatial scale) forcing, we note that our results do not exhibit a regime change at strong forcing as found by Wang et al. (2012).

4. Discussion

It is illuminating to compare these results with some of the previous literature in more detail. This section informs as to the robustness of results, by comparing this model to others, and also indicates where previous

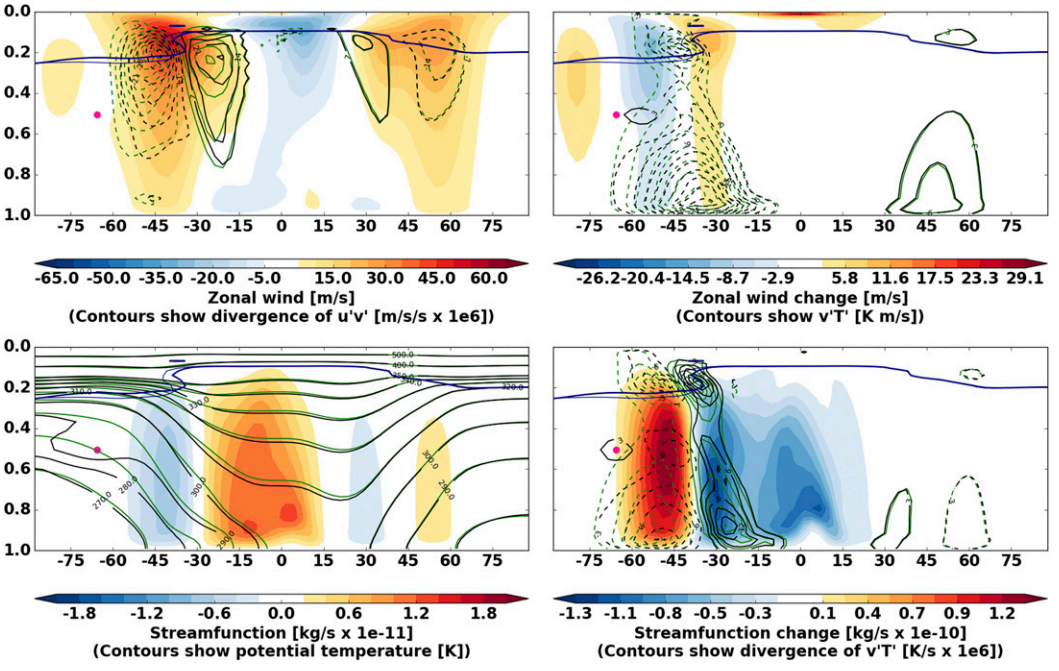

FIG. 9. Case 3: As in Fig. 7, but for heating applied at $\sigma = 0.5$ and $\phi = -66°$ (pink dot).

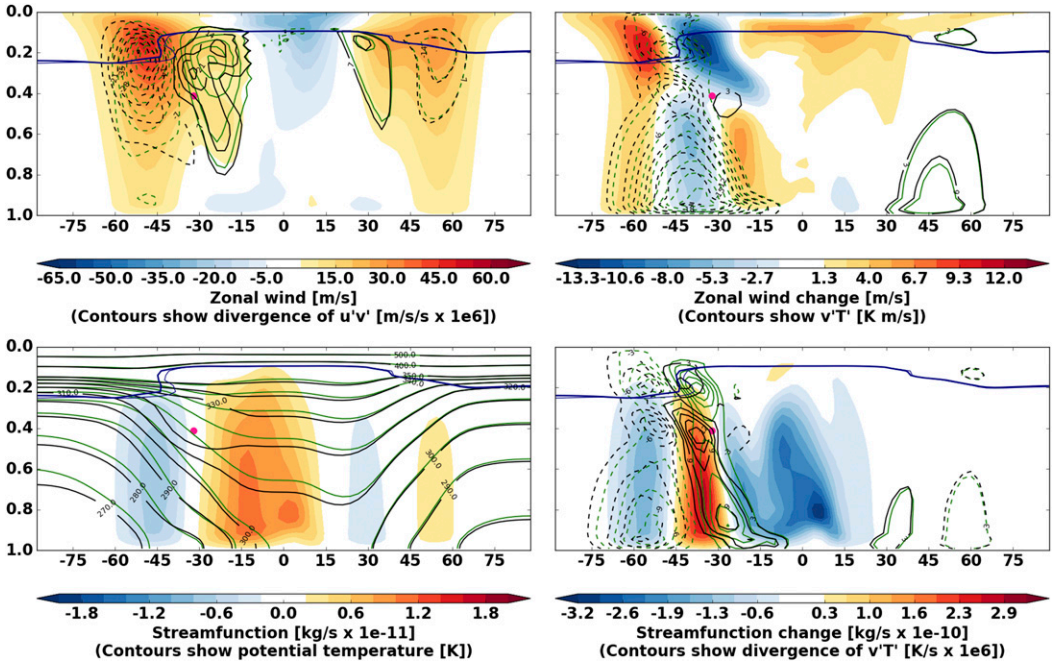

FIG. 10. Case 4: As in Fig. 7, but for heating applied at $\sigma = 0.4$ and $\phi = -32°$ (pink dot).

results can be interpreted in the context of the sensitivities described here.

Early work by Son and Lee (2005) used a dry idealized model with tropical heating and polar cooling. Applying heating in a very narrow band across the equator throughout the depth of troposphere produces a marginal equatorward shift of the jet, and a strengthening of the jet (their Fig. 4). Polar cooling acts to shift the jet poleward

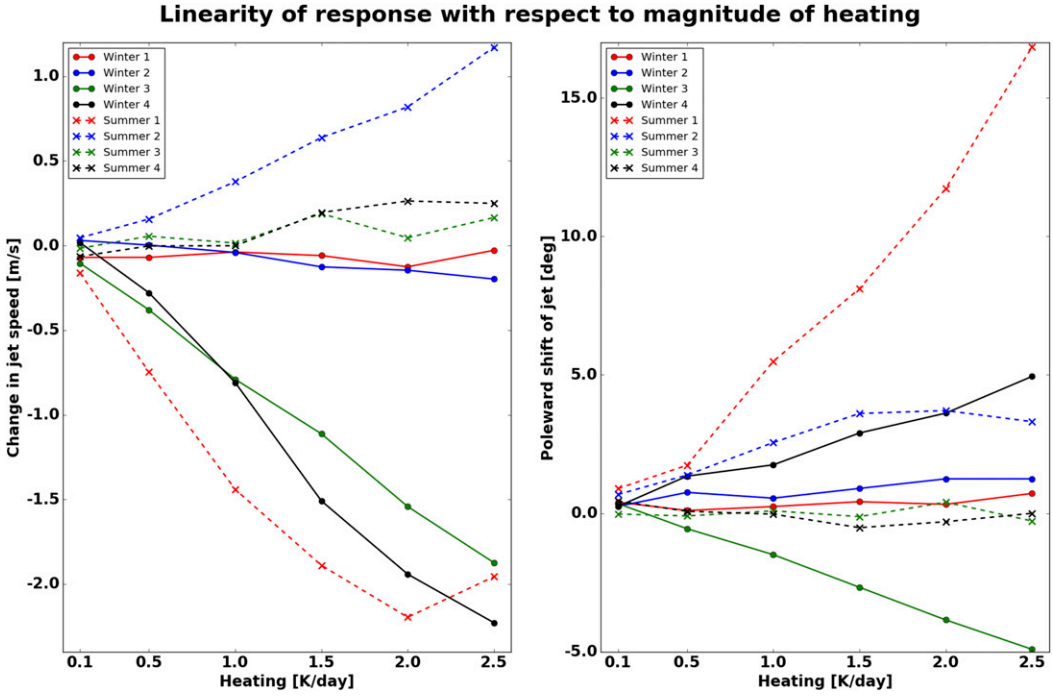

FIG. 11. (left) Change in jet speed for each of the four case studies in winter and summer as q_0 varies. (right) Poleward jet shift for each of the four case studies in winter and summer as q_0 varies. Solid lines indicate winter jet responses; dashed lines indicate summer jet responses.

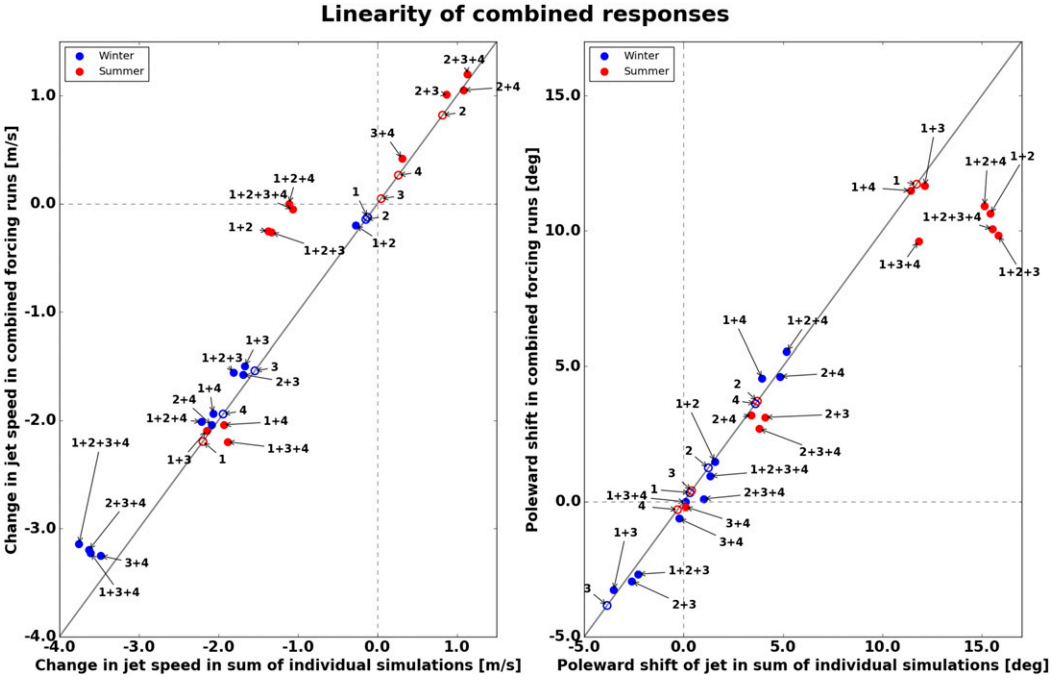

FIG. 12. (left) Scatter graph showing the change in jet speed in simulations where the forcings used in the case studies are combined against linear combinations of the results from each individual case study. (right) Scatter graph showing the poleward jet shift in simulations where the forcings used in the case studies are combined against linear combinations of the results from each individual case study. Blue points indicate winter jet responses; red points indicate summer jet responses, with open circles representing the changes in the sole forcing cases. The labels indicate which case study forcings have been combined at that particular point. In all simulations, $q_0 = 2.0$ K day^{-1}.

and marginally weaken the jet. These findings are consistent with the sensitivities found in this study, aside from the jet weakening due to polar cooling (assuming that a cooling at the pole produces an equivalent magnitude but opposite sign response to polar heating). Son and Lee (2005) also performed a set of moist runs to investigate the effect of latent heating on the jet, removing their heating and cooling thermal forcing so the latent heating is the only forcing. Because much of the effect of moisture manifests in the tropics, the impact is similar to adding the tropical heating thermal forcing. This demonstrates the utility of dry idealized models in developing understanding of the jet response to thermal forcings.

One important result from the sensitivity findings is that the response of the climate to thermal forcing will depend strongly on the position of the thermal forcing. Butler et al. (2010) apply thermal forcings in a dry idealized model and yet find, in direct contrast to Son and Lee (2005), that the response to their tropical heating produces a poleward shift of the jet (their Figs. 2, 6, and 7). The same is also true of McGraw and Barnes (2016), who find a poleward jet shift due to tropical heating (their Fig. 3). As shown by Fig. 3 herein, the poleward extent of the tropical heating has an important effect on whether the shift is poleward or equatorward. If the heating is confined near to the equator, Fig. 3 indicates that the response should be an equatorward shift. As the extent of the heating broadens, it will start to impinge on the zone where a heating will cause a poleward shift, and so the shape of the forcing will determine which of the two competing effects will dominate to determine the direction of shift. Sun et al. (2013) and Tandon et al. (2013) observe similar sensitivities with regard to the direction of jet latitude shift depending on the spatial extent of the thermal forcing. Tandon et al. (2013) suggest that this dependence is due to the Hadley cell edge shifting toward the anomalous diabatic cooling on the flank of the positive thermal forcing. Lu et al. (2008) examine the circulation responses in CMIP3 models to El Niño versus global warming. The typical El Niño response is an equatorward shift of the jet, as opposed to the anticipated poleward shift and strengthening under global warming. The sensitivities found in this study are again consistent with this difference in response. As the El Niño SST pattern is centered on the equator, with narrow poleward extent, the response seen is due to the weakening in the Hadley cell coupled with an increase in latent heating due to increased precipitation over the equator.

The difference in sensitivity of the speed and latitude highlights the importance of moving away from the

NAO or annular mode view to examine circulation changes in the midlatitudes. Lorenz and DeWeaver (2007) use the first EOF of zonal wind to characterize the sensitivity of the jet, and in doing so produce a sensitivity plot that is an amalgamation of the two jet indices (their Fig. 9). This inhibits the ability to draw conclusions about the changes in the jet and the mechanisms behind these. Despite this, their results do broadly agree with the sensitivities in this study: heating equatorward of the jet causes a poleward shift, and heating poleward of the jet causes an equatorward shift (since the annular modes in zonally symmetric models tend to reflect changes in jet latitude primarily). Heating near the surface at 60°N produces a large equatorward shift in the jet, and the largest poleward shift comes from heating at 300 hPa in the subtropics. As shown in this study, different mechanisms are responsible for driving the different changes in the jet; therefore, to accurately quantify and understand the response, the separate characteristics of the jet must be considered individually, not as an annular mode.

The variation in seasonal sensitivity indicates that the jet latitude is more sensitive in summer, and the jet speed more so in winter. This is demonstrated by the fact that the summer jet displays the largest shift in latitude, and the winter jet experiences the greatest jet speed amplitude change. Although the results in this study are just the sensitivities and not responses, this seems to be corroborated by predictions from the CMIP5 models, which predict a poleward shift of the North Atlantic jet in summer, and a strengthening and lengthening in winter (Barnes and Polvani 2013). McGraw and Barnes (2016) investigate the jet response to a climate change–like forcing using a dry idealized model. They find that combined high tropical tropospheric and surface polar forcings produce a larger poleward shift in winter and a weakening of the jet in both summer and winter. This could be different from the CMIP5 responses as the positions of the forcings may not be concurrent with those in the CMIP5 models, and it again highlights the importance of understanding the jet sensitivities and the exact thermal forcing due to anthropogenic warming. Understanding the spatial position and extent of the thermal forcing is not trivial; as well as direct forcing due to radiative effects due to CO_2, cloud feedbacks also act to alter diabatic heating in the atmosphere, and this has been shown to have an impact on the jets (e.g., Voigt and Shaw 2015; Ceppi and Hartmann 2016; Tandon and Cane 2017). This highlights the importance of the sensitivity results presented in this study, as these cloud feedbacks may not necessarily manifest in the tropical upper troposphere and Arctic where the radiative and Arctic amplification warmings occur due to anthropogenic global warming.

The mechanism postulated in this study acts through the changes in isentropic surfaces, with changes in low-level meridional temperature gradients affecting the jet. Brayshaw et al. (2008) investigated the effect of changing the surface gradients through applying SST perturbations. Increased SST gradients in the subtropics caused an equatorward shift and strengthening of the storm track and vice versa for decreased gradients. Increasing SST gradients in the midlatitudes caused a poleward shift and strengthening of the storm track and vice versa for decreased gradients (their Table 2). The strengthening of the storm track agrees with the results found in this study; by increasing the temperature gradient from equator to pole, the jet strengthens. Brayshaw et al. (2008) attribute the changes due to midlatitude gradients to lower-tropospheric baroclinicity, with the increase in midlatitude gradients strengthening the baroclinicity around the jet and shifting the maximum poleward with the storm track. The equatorward shift of the storm track in Brayshaw et al. (2008) is attributed to a weakening in the tropically driven component of the Hadley cell, thus shifting the maximum in temperature gradient equatorward and the storm track too. This shifting mechanism does not preclude the strengthening of the storm track or jet, which can indeed be seen in certain cases in this study where the jet does shift equatorward. Graff and LaCasce (2012) also perform experiments altering the SST gradients in the tropics and midlatitudes and come to the same conclusion.

The sensitivities determined here can be used to explain results found in more complex models. One of the conclusions from the sensitivity analysis is that heating has to be applied poleward of the storm track in order to weaken the jet, and there is a sharp edge to this region of sensitivity. Conversely, assuming signs can be reversed, a strengthening of the jet could arise due to a cooling, provided this occurs poleward of the storm track. This suggests that the sensitivity of the Atlantic storm track to weakening of the Atlantic meridional overturning circulation (Woollings et al. 2012) might be caused by cooling in the Nordic seas region, rather than in the subpolar gyre farther south (see also Harvey et al. 2015). Note also that in this example, regional jet changes could be forced from the tropics via a Rossby wave mechanism (Ciasto et al. 2016).

The implications of this study reach beyond that of climate change alone. Our results can also aid understanding of jet changes due to natural variability. The sensitivities are also in line with results from studies that use reanalyses to draw insights into changes in the jet. For example, Hall et al. (2017) perform a multiple linear regression to determine drivers of the North Atlantic

eddy-driven jet in summer. Many of the predictors they find to be significant (see their Table 1) can be explained from the sensitivities determined in this study. For instance, they suggest that the El Niño (see previous discussion) and winter AMO (see discussion below) could act to drive the jet equatorward; increases in the Barents–Kara Sea ice and increases in the Atlantic SST tripole could drive the jet poleward; and increases in tripole SST and tropical rainfall could strengthen the jet. Increasing sea ice acts as a cooling, so a poleward shift agrees with the sensitivity over the pole to thermal forcing as found in this study (see Fig. 3). An increase in their tripole SST index increases the equator-to-pole temperature contrast. As indicated by the mechanisms discussed in this study, this should strengthen the jet, and could cause the position of the low-level temperature gradient maximum to shift, causing the jet shift. Increases in rainfall imply greater latent heat release, which agrees with our finding that an increase in thermal forcing in the tropics acts to strengthen the jet.

Focusing more on the AMO, Peings and Magnusdottir (2014) show that an increase in the AMO can force a negative NAO response in winter. This likely reflects an equatorward shift of the jet, as also seen in summer (Sutton and Dong 2012). There is debate over whether and where the AMO does force the atmosphere. Gulev et al. (2013) show that the positive heat fluxes from the AMO correspond to an increase in temperature over the midlatitudes, suggesting that in the midlatitudes the ocean drives the atmosphere. However, Davini et al. (2015) argue that the effect on the atmosphere from the AMO arises from forcing in the tropics, with little influence from the extratropics. From the sensitivities in this study, it seems that the ocean could force an equatorward jet shift due to warming in the middle and high latitudes on the poleward flank of the jet, or the deep tropics, and not the subtropics/midlatitudes on the equatorward jet flank. Clearly, the results from the dry model do not necessarily explain all the facets of the problem, but they do allow insights to be made as to where the AMO may be forcing the atmosphere.

Another use for the sensitivities in this study is to aid in assessing sensitivity to model biases in the position of diabatic heating. For example, Hawcroft et al. (2017) identify likely biases in the distribution of latent heating in both the High-Resolution Global Environmental Model (HiGEM) and the ERA-Interim reanalysis. Given the uncertainty in the true distribution of atmospheric latent heating, it is advisable to be aware of the sensitivity of the circulation to the location of heating. One general conclusion from this study is that the atmosphere might be more sensitive to biases in the latitude of the heating than in its height.

5. Conclusions

In this study, the sensitivity of the eddy-driven jet in a North Atlantic–like background state has been examined in an idealized dry GCM using a series of thermally forced simulations. The model was set up to allow the sensitivity in both summer and winter to be studied by keeping each hemisphere in a perpetual seasonal state.

The main findings in these experiments are the following:

1) The speed and latitude of the jet display different sensitivities to thermal forcing. This means that treating the response of the jet under forcing as simply a change in NAO or annular mode index will not capture the full response. It also means that the speed and latitude of the jet are affected by different mechanisms in responding to thermal forcing.
2) The sensitivity of the jet varies between winter and summer. Latitude shift sensitivities are highest in the midlatitudes and polar regions near to the jet core, and these sensitivities move poleward in summer. Jet speed sensitivities extend more prominently into the subtropics and tropics. The winter jet latitude, however, is affected by heating in the summer hemisphere.
3) The sensitivities of the storm track closely match those of the jet, suggesting that the two shift and strengthen in near tandem in response to forcing. Understanding how the jet will respond is therefore vital in understanding how midlatitude weather will be affected.
4) The variability of the jet, as quantified in this study by the jet spread measure, is shown to broadly increase with heating in the jet core and on the equatorward flank of the jet, but decrease when forced in the polar region. Changes in spread are consistent with changes in the baroclinic zone width and low-level meridional temperature gradient, with an increase in spread due to an increase in baroclinic zone width and/or meridional temperature gradient, and a decrease due to a decrease in baroclinic zone width and/or meridional temperature gradient.
5) In the case studies examined, the responses of latitude and speed scale approximately linearly with the strength and combination of forcings applied. This is especially clear for the winter cases.

The proposed mechanisms for the sensitivities determined in this study come from changes in the slopes of isentropic surfaces and hence in the location and strength of the strongest low-level horizontal temperature

gradients [as in Butler et al. (2011)]. Shifts of the jet are driven by changes in the position of the maximum low-level meridional temperature gradient, which determines where the maximum meridional heat flux occurs. Changes in jet strength arise from changes in the low-level meridional temperature gradient across the storm track, which dictates the amount of meridional heat flux.

Understanding the jet sensitivities is the first step toward understanding the effects of climate change on the midlatitudes. Given the uncertainty in the distribution of thermal forcing, knowledge of the sensitivity of the dynamics to forcing location provides guidance on how uncertainty in the circulation response could be reduced. Areas where the uncertainty of the anthropogenic forcing is high and the sensitivity of the jet is high (e.g., in the tropical upper troposphere) are clearly areas that need further study to better constrain the position and size of the expected anthropogenic forcing.

Acknowledgments. This work was supported by the Natural Environment Research Council (Grant NE/L002612/1 and NERC SummerTIME project, Grant NE/M005887/1), and the Research Council of Norway project jetSTREAM (Grant 231716). The authors thank the three anonymous reviewers, whose comments have improved this manuscript.

REFERENCES

Allen, R. J., S. C. Sherwood, J. R. Norris, and C. S. Zender, 2012: The equilibrium response to idealized thermal forcings in a comprehensive GCM: Implications for recent tropical expansion. *Atmos. Chem. Phys.*, **12**, 4795–4816, doi:10.5194/acp-12-4795-2012.

Baldwin, M. P., D. B. Stephenson, D. W. J. Thompson, T. J. Dunkerton, A. J. Charlton, and A. O'Neill, 2003: Stratospheric memory and skill of extended-range weather forecasts. *Science*, **301**, 636–640, doi:10.1126/science.1087143.

Barnes, E. A., and D. L. Hartmann, 2011: Rossby wave scales, propagation, and the variability of eddy-driven jets. *J. Atmos. Sci.*, **68**, 2893–2908, doi:10.1175/JAS-D-11-039.1.

——, and L. Polvani, 2013: Response of the midlatitude jets, and of their variability, to increased greenhouse gases in the CMIP5 models. *J. Climate*, **26**, 7117–7135, doi:10.1175/JCLI-D-12-00536.1.

Brayshaw, D. J., B. Hoskins, and M. Blackburn, 2008: The storm-track response to idealized SST perturbations in an aquaplanet GCM. *J. Atmos. Sci.*, **65**, 2842–2860, doi:10.1175/2008JAS2657.1.

Burrows, D. A., G. Chen, and L. Sun, 2017: Barotropic and baroclinic eddy feedbacks in the midlatitude jet variability and responses to climate change–like thermal forcings. *J. Atmos. Sci.*, **74**, 111–132, doi:10.1175/JAS-D-16-0047.1.

Butler, A. H., D. W. J. Thompson, and R. Heikes, 2010: The steady-state atmospheric circulation response to climate change-like thermal forcings in a simple general circulation model. *J. Climate*, **23**, 3474–3496, doi:10.1175/2010JCLI3228.1.

——, ——, and T. Birner, 2011: Isentropic slopes, downgradient eddy fluxes, and the extratropical atmospheric circulation response to tropical tropospheric heating. *J. Atmos. Sci.*, **68**, 2292–2305, doi:10.1175/JAS-D-10-05025.1.

Ceppi, P., and D. L. Hartmann, 2016: Clouds and the atmospheric circulation response to warming. *J. Climate*, **29**, 783–799, doi:10.1175/JCLI-D-15-0394.1.

Chan, C. J., and R. A. Plumb, 2009: The response to stratospheric forcing and its dependence on the state of the troposphere. *J. Atmos. Sci.*, **66**, 2107–2115, doi:10.1175/2009JAS2937.1.

Chen, G., and I. M. Held, 2007: Phase speed spectra and the recent poleward shift of Southern Hemisphere surface westerlies. *Geophys. Res. Lett.*, **34**, L21805, doi:10.1029/2007GL031200.

——, J. Lu, and D. M. W. Frierson, 2008: Phase speed spectra and the latitude of surface westerlies: Interannual variability and global warming trend. *J. Climate*, **21**, 5942–5959, doi:10.1175/2008JCLI2306.1.

Ciasto, L. M., C. Li, J. J. Wettstein, and N. G. Kvamstø, 2016: North Atlantic storm-track sensitivity to projected sea surface temperature: Local versus remote influences. *J. Climate*, **29**, 6973–6991, doi:10.1175/JCLI-D-15-0860.1.

Davini, P., J. von Hardenberg, and S. Corti, 2015: Tropical origin for the impacts of the Atlantic multidecadal variability on the Euro-Atlantic climate. *Environ. Res. Lett.*, **10**, 094010, doi:10.1088/1748-9326/10/9/094010.

Deser, C., R. Tomas, M. Alexander, and D. Lawrence, 2010: The seasonal atmospheric response to projected Arctic sea ice loss in the late twenty-first century. *J. Climate*, **23**, 333–351, doi:10.1175/2009JCLI3053.1.

——, A. Phillips, V. Bourdette, and H. Teng, 2012: Uncertainty in climate change projections: The role of internal variability. *Climate Dyn.*, **38**, 527–546, doi:10.1007/s00382-010-0977-x.

Edmon, H. J., B. J. Hoskins, and M. E. McIntyre, 1980: Eliassen–Palm cross sections for the troposphere. *J. Atmos. Sci.*, **37**, 2600–2616, doi:10.1175/1520-0469(1980)037<2600:EPCSFT>2.0.CO;2.

Francis, J. A., and S. J. Vavrus, 2012: Evidence linking Arctic amplification to extreme weather in mid-latitudes. *Geophys. Res. Lett.*, **39**, L06801, doi:10.1029/2012GL051000.

Frierson, D. M. W., 2008: Midlatitude static stability in simple and comprehensive general circulation models. *J. Atmos. Sci.*, **65**, 1049–1062, doi:10.1175/2007JAS2373.1.

Garfinkel, C. I., D. W. Waugh, and E. P. Gerber, 2013: The effect of tropospheric jet latitude on coupling between the stratospheric polar vortex and the troposphere. *J. Climate*, **26**, 2077–2095, doi:10.1175/JCLI-D-12-00301.1.

Gerber, E. P., and G. K. Vallis, 2007: Eddy–zonal flow interactions and the persistence of the zonal index. *J. Atmos. Sci.*, **64**, 3296–3311, doi:10.1175/JAS4006.1.

——, and L. M. Polvani, 2009: Stratosphere–troposphere coupling in a relatively simple AGCM: The importance of stratospheric variability. *J. Climate*, **22**, 1920–1933, doi:10.1175/2008JCLI2548.1.

——, S. Voronin, and L. M. Polvani, 2008: Testing the annular mode autocorrelation time scale in simple atmospheric general circulation models. *Mon. Wea. Rev.*, **136**, 1523–1536, doi:10.1175/2007MWR2211.1.

Graff, L. S., and J. H. LaCasce, 2012: Changes in the extratropical storm tracks in response to changes in SST in an AGCM. *J. Climate*, **25**, 1854–1870, doi:10.1175/JCLI-D-11-00174.1.

Grise, K. M., and L. M. Polvani, 2016: Is climate sensitivity related to dynamical sensitivity? *J. Geophys. Res. Atmos.*, **121**, 5159–5176, doi:10.1002/2015JD024687.

Gulev, S. K., M. Latif, N. Keenlyside, W. Park, and K. P. Koltermann, 2013: North Atlantic Ocean control on surface heat flux on multidecadal timescales. *Nature*, **499**, 464–467, doi:10.1038/nature12268.

Hall, R. J., J. M. Jones, E. Hanna, A. A. Scaife, and R. Erdélyi, 2017: Drivers and potential predictability of summer time North Atlantic polar front jet variability. *Climate Dyn.*, **48**, 3869–3887, doi:10.1007/s00382-016-3307-0.

Hannachi, A., E. A. Barnes, and T. Woollings, 2013: Behaviour of the winter North Atlantic eddy-driven jet stream in the CMIP3 integrations. *Climate Dyn.*, **41**, 995–1007, doi:10.1007/s00382-012-1560-4.

Harvey, B. J., L. C. Shaffrey, and T. J. Woollings, 2015: Deconstructing the climate change response of the Northern Hemisphere wintertime storm tracks. *Climate Dyn.*, **45**, 2847–2860, doi:10.1007/s00382-015-2510-8.

Hassanzadeh, P., and Z. Kuang, 2016: The linear response function of an idealized atmosphere. Part I: Construction using Green's functions and applications. *J. Atmos. Sci.*, **73**, 3423–3439, doi:10.1175/JAS-D-15-0338.1.

Hawcroft, M., H. Dacre, R. Forbes, K. Hodges, L. Shaffrey, and T. Stein, 2017: Using satellite and reanalysis data to evaluate the representation of latent heating in extratropical cyclones in a climate model. *Climate Dyn.*, **48**, 2255–2278, doi:10.1007/s00382-016-3204-6.

Held, I. M., 2007: Progress and problems in large-scale atmospheric dynamics. *Global Circulation of the Atmosphere*, T. Schneider and A. H. Sobel, Eds., Princeton University Press, 1–21.

Hoskins, B. J., and P. J. Valdes, 1990: On the existence of storm-tracks. *J. Atmos. Sci.*, **47**, 1854–1864, doi:10.1175/1520-0469(1990)047<1854:OTEOST>2.0.CO;2.

IPCC, 2013: *Climate Change 2013: The Physical Science Basis*. Cambridge University Press, 1535 pp.

Karpechko, A. Y., 2010: Uncertainties in future climate attributable to uncertainties in future northern annular mode trend. *Geophys. Res. Lett.*, **37**, L20702, doi:10.1029/2010GL044717.

Keeley, S. P. E., R. T. Sutton, and L. C. Shaffrey, 2009: Does the North Atlantic Oscillation show unusual persistence on intraseasonal timescales? *Geophys. Res. Lett.*, **36**, L22706, doi:10.1029/2009GL040367.

Kidston, J., and E. P. Gerber, 2010: Intermodel variability of the poleward shift of the austral jet stream in the CMIP3 integrations linked to biases in 20th century climatology. *Geophys. Res. Lett.*, **37**, L09708, doi:10.1029/2010GL042873.

——, S. M. Dean, J. A. Renwick, and G. K. Vallis, 2010: A robust increase in the eddy length scale in the simulation of future climates. *Geophys. Res. Lett.*, **37**, L03806, doi:10.1029/2009GL041615.

Kim, B.-M., S.-W. Son, S.-K. Min, J.-H. Jeong, S.-J. Kim, X. Zhang, T. Shim, and J.-H. Yoon, 2014: Weakening of the stratospheric polar vortex by Arctic sea-ice loss. *Nat. Commun.*, **5**, 4646, doi:10.1038/ncomms5646.

Kushner, P. J., and L. M. Polvani, 2004: Stratosphere–troposphere coupling in a relatively simple AGCM: The role of eddies. *J. Climate*, **17**, 629–639, doi:10.1175/1520-0442(2004)017<0629:SCIARS>2.0.CO;2.

Lorenz, D. J., 2014: Understanding midlatitude jet variability and change using Rossby wave chromatography: Poleward-shifted jets in response to external forcing. *J. Atmos. Sci.*, **71**, 2370–2389, doi:10.1175/JAS-D-13-0200.1.

——, and E. T. DeWeaver, 2007: Tropopause height and zonal wind response to global warming in the IPCC scenario integrations. *J. Geophys. Res.*, **112**, D10119, doi:10.1029/2006JD008087.

Lu, J., G. Chen, and D. M. W. Frierson, 2008: Response of the zonal mean atmospheric circulation to El Niño versus global warming. *J. Climate*, **21**, 5835–5851, doi:10.1175/2008JCLI2200.1.

——, ——, and ——, 2010: The position of the midlatitude storm track and eddy-driven westerlies in aquaplanet AGCMs. *J. Atmos. Sci.*, **67**, 3984–4000, doi:10.1175/2010JAS3477.1.

——, L. Sun, Y. Wu, and G. Chen, 2014: The role of subtropical irreversible PV mixing in the zonal mean circulation response to global warming–like thermal forcing. *J. Climate*, **27**, 2297–2316, doi:10.1175/JCLI-D-13-00372.1.

Manzini, E., and Coauthors, 2014: Northern winter climate change: Assessment of uncertainty in CMIP5 projections related to stratosphere–troposphere coupling. *J. Geophys. Res. Atmos.*, **119**, 7979–7998, doi:10.1002/2013JD021403.

Mbengue, C., and T. Schneider, 2013: Storm track shifts under climate change: What can be learned from large-scale dry dynamics. *J. Climate*, **26**, 9923–9930, doi:10.1175/JCLI-D-13-00404.1.

——, and ——, 2017: Storm-track shifts under climate change: Toward a mechanistic understanding using baroclinic mean available potential energy. *J. Atmos. Sci.*, **74**, 93–110, doi:10.1175/JAS-D-15-0267.1.

McGraw, M. C., and E. A. Barnes, 2016: Seasonal sensitivity of the eddy-driven jet to tropospheric heating in an idealized AGCM. *J. Climate*, **29**, 5223–5240, doi:10.1175/JCLI-D-15-0723.1.

Mitchell, D. M., L. J. Gray, J. Anstey, M. P. Baldwin, and A. J. Charlton-Perez, 2013: The influence of stratospheric vortex displacements and splits on surface climate. *J. Climate*, **26**, 2668–2682, doi:10.1175/JCLI-D-12-00030.1.

Monahan, A. H., and J. C. Fyfe, 2006: On the nature of zonal jet EOFs. *J. Climate*, **19**, 6409–6424, doi:10.1175/JCLI3960.1.

Peings, Y., and G. Magnusdottir, 2014: Forcing of the wintertime atmospheric circulation by the multidecadal fluctuations of the North Atlantic Ocean. *Environ. Res. Lett.*, **9**, 034018, doi:10.1088/1748-9326/9/3/034018.

Petrie, R. E., L. C. Shaffrey, and R. T. Sutton, 2015: Atmospheric impact of Arctic sea ice loss in a coupled ocean–atmosphere simulation. *J. Climate*, **28**, 9606–9622, doi:10.1175/JCLI-D-15-0316.1.

Polvani, L. M., and P. J. Kushner, 2002: Tropospheric response to stratospheric perturbations in a relatively simple general circulation model. *Geophys. Res. Lett.*, **29**, 1114, doi:10.1029/2001GL014284.

Ring, M. J., and R. A. Plumb, 2008: The response of a simplified GCM to axisymmetric forcings: Applicability of the fluctuation–dissipation theorem. *J. Atmos. Sci.*, **65**, 3880–3898, doi:10.1175/2008JAS2773.1.

Rivière, G., 2011: A dynamical interpretation of the poleward shift of the jet streams in global warming scenarios. *J. Atmos. Sci.*, **68**, 1253–1272, doi:10.1175/2011JAS3641.1.

Schneider, T., 2004: The tropopause and the thermal stratification in the extratropics of a dry atmosphere. *J. Atmos. Sci.*, **61**, 1317–1340, doi:10.1175/1520-0469(2004)061<1317:TTATTS>2.0.CO;2.

——, 2007: The thermal stratification of the extratropical troposphere. *Global Circulation of the Atmosphere*, T. Schneider and A. H. Sobel, Eds., Princeton University Press, 47–77.

——, and C. C. Walker, 2006: Self-organization of atmospheric macroturbulence into critical states of weak nonlinear eddy–eddy interactions. *J. Atmos. Sci.*, **63**, 1569–1586, doi:10.1175/JAS3699.1.

Shaw, T. A., and A. Voigt, 2015: Tug of war on summertime circulation between radiative forcing and sea surface warming. *Nat. Geosci.*, **8**, 560–566, doi:10.1038/ngeo2449.

——, and Coauthors, 2016: Storm track processes and the opposing influences of climate change. *Nat. Geosci.*, **9**, 656–664, doi:10.1038/ngeo2783.

Sheshadri, A., and R. A. Plumb, 2017: Propagating annular modes: Empirical orthogonal functions, principal oscillation patterns, and time scales. *J. Atmos. Sci.*, **74**, 1345–1361, doi:10.1175/JAS-D-16-0291.1.

Simpson, I. R., T. A. Shaw, and R. Seager, 2014: A diagnosis of the seasonally and longitudinally varying midlatitude circulation response to global warming. *J. Atmos. Sci.*, **71**, 2489–2515, doi:10.1175/JAS-D-13-0325.1.

Son, S.-W., and S. Lee, 2005: The response of westerly jets to thermal driving in a primitive equation model. *J. Atmos. Sci.*, **62**, 3741–3757, doi:10.1175/JAS3571.1.

——, N. F. Tandon, L. M. Polvani, and D. W. Waugh, 2009: Ozone hole and Southern Hemisphere climate change. *Geophys. Res. Lett.*, **36**, L15705, doi:10.1029/2009GL038671.

Sun, L., G. Chen, and J. Lu, 2013: Sensitivities and mechanisms of the zonal mean atmospheric circulation response to tropical warming. *J. Atmos. Sci.*, **70**, 2487–2504, doi:10.1175/JAS-D-12-0298.1.

——, C. Deser, and R. A. Tomas, 2015: Mechanisms of stratospheric and tropospheric circulation response to projected Arctic sea ice loss. *J. Climate*, **28**, 7824–7845, doi:10.1175/JCLI-D-15-0169.1.

Sutton, R., and B. Dong, 2012: Atlantic Ocean influence on a shift in European climate in the 1990s. *Nat. Geosci.*, **5**, 788–792, doi:10.1038/ngeo1595.

Tandon, N. F., and M. A. Cane, 2017: Which way will the circulation shift in a changing climate? Possible nonlinearity of extratropical cloud feedbacks. *Climate Dyn.*, **48**, 3759–3777, doi:10.1007/s00382-016-3301-6.

——, E. P. Gerber, A. H. Sobel, and L. M. Polvani, 2013: Understanding Hadley cell expansion versus contraction: Insights from simplified models and implications for recent observations. *J. Climate*, **26**, 4304–4321, doi:10.1175/JCLI-D-12-00598.1.

Vallis, G. K., E. P. Gerber, P. J. Kushner, and B. A. Cash, 2004: A mechanism and simple dynamical model of the North Atlantic Oscillation and annular modes. *J. Atmos. Sci.*, **61**, 264–280, doi:10.1175/1520-0469(2004)061<0264:AMASDM>2.0.CO;2.

Voigt, A., and T. A. Shaw, 2015: Circulation response to warming shaped by radiative changes of clouds and water vapour. *Nat. Geosci.*, **8**, 102–106, doi:10.1038/ngeo2345.

Wang, S., E. P. Gerber, and L. M. Polvani, 2012: Abrupt circulation responses to tropical upper-tropospheric warming in a relatively simple stratosphere-resolving AGCM. *J. Climate*, **25**, 4097–4115, doi:10.1175/JCLI-D-11-00166.1.

Woollings, T., B. Hoskins, M. Blackburn, and P. Berrisford, 2008: A new Rossby wave-breaking interpretation of the North Atlantic Oscillation. *J. Atmos. Sci.*, **65**, 609–626, doi:10.1175/2007JAS2347.1.

——, A. Hannachi, and B. Hoskins, 2010: Variability of the North Atlantic eddy-driven jet stream. *Quart. J. Roy. Meteor. Soc.*, **136**, 856–868, doi:10.1002/qj.625.

——, J. M. Gregory, J. G. Pinto, M. Reyers, and D. J. Brayshaw, 2012: Response of the North Atlantic storm track to climate change shaped by ocean–atmosphere coupling. *Nat. Geosci.*, **5**, 313–317, doi:10.1038/ngeo1438.

——, L. Papritz, C. Mbengue, and T. Spengler, 2016: Diabatic heating and jet stream shifts: A case study of the 2010 negative North Atlantic Oscillation winter. *Geophys. Res. Lett.*, **43**, 9994–10 002, doi:10.1002/2016GL070146.

Yin, J. H., 2005: A consistent poleward shift of the storm tracks in simulations of 21st century climate. *Geophys. Res. Lett.*, **32**, L18701, doi:10.1029/2005GL023684.